ACADEMIC PRESS

Available online at www.sciencedirect.com

SCIENCE DIRECT®

Journal of Sound and Vibration 264 (2003) 177–201

JOURNAL OF SOUND AND VIBRATION

www.elsevier.com/locate/jsvi

Parametric control of an axially moving string via fuzzy sliding-mode and fuzzy neural network methods

Jeng-Sheng Huang[a], Paul C.-P. Chao[a,*], Rong-Fong Fung[b], Cheng-Liang Lai[a]

[a] *Department of Mechanical Engineering, Chung Yuan Christian University, Chung-Li, 32023 Taiwan, ROC*
[b] *Department of Mechanical and Automation Engineering, National Kaohsiung First University of Science and Technology, Kaohsiung, Taiwan, ROC*

Received 20 February 2001; accepted 31 July 2002

Abstract

This study is dedicated to design effective control schemes to suppress transverse vibration of an axially moving string system by adjusting the axial tension of the string. To this end, a continuous model in the form of partial differential equations is first established to describe the system dynamics. Using an energy-like system functional as a Lyapunov function, a sliding-mode controller (SMC) is designed to be applied when the level of vibration is not small. Due to non-analyticity of the SMC control effort generated as vibration level becoming small, two intelligent control schemes are proposed to complete the task — fuzzy sliding-mode control (FSMC) and fuzzy neural network control (FNNC). Both control approaches are based on a common structure of fuzzy control, taking switching function and its derivative as inputs and tension variation as output to reduce the transverse vibration of the string. In the framework of FSMC, genetic algorithm (GA) is utilized to search for the optimal scalings for the inputs; in addition, the technique of regionwise linear fuzzy logic control (RLFLC) is employed to simplify the computation procedure of the fuzzy reasoning. On the other hand, FNNC is proposed for conducting on-line tuning of control parameters to overcome model uncertainty. Numerical simulations are conducted to verify the effectiveness of controllers. Satisfactory stability and vibration suppression are attained for all controllers with the findings that the FSMC assisted by GA holds the advantage of fast convergence with a precise model while the FNNC is robust to model uncertainty and environmental disturbance although a relatively slower convergence could be present.

*Corresponding author. Fax: 886-3-2654399.
E-mail addresses: jengshen@cycu.edu.tw (J.-S. Huang), pchao@cycu.edu.tw (P.C.-P. Chao).

0022-460X/03/$ - see front matter
doi:10.1016/S0022-460X(02)01196-3

1. Introduction

An axially moving string system is often utilized to represent various realistic mechanical systems such as travelling strings, magnetic tapes, band saws and cable tramways, etc. Early research was focused on analyzing vibrations of the system [1–3] to understand the basic dynamic characteristics. Other than dynamics analysis, active vibration suppression of the axially moving string was an intensive topic for many industrial applications. Researchers initially conducted vibration suppression by the so-called "modal control," which first approximates the string by a set of discrete. vibratory modes and then applies the existing control techniques to synthesize controllers [4–6]. Some researchers instead used the finite-dimensional modelling to approximate the original continuous string system for designing the controller [7–14]. In recent years, Rahn and Mote [15–17] have proposed "parametric control" to mechanical systems, which refers to the control schemes that activate on-line adjustment of some system parameters to achieve pre-designated control goals. As it is applied to flexible, continuous systems, the objective is usually to achieve satisfactory vibration suppression.

In the present study, the essence of the parametric control, utilizing variation of string tension, is adopted to design various controllers for suppressing the transverse vibration of an axially moving string. The design process starts, in Section 2, by establishing a continuous mathematical model of an axially moving string used for describing transverse vibrations of the string system. A conventional sliding-mode controller (SMC) [18] is designed in Section 3 by considering the energy-like system functional as a Lyapunov function, with which related stability analysis can be conducted. To avoid non-analyticity of the designed SMC as the level of the vibration becomes small intelligent controllers are proposed in Section 4, to complement the SMC in a prescribed boundary layer near the switching surface, forming a hybrid control design. The proposed complementary controllers are based on the mechanism of fuzzy logic control (FLC). The FLC is built based on the theory of fuzzy sets, which were first introduced by Zadeh in 1965 [19]. The first successful application of fuzzy sets theory in the control field was presented by Mamdani in 1974 [20]. In designing a FLC, some common difficulties are encountered; such as (1) inference rules are model dependent and experience oriented; thus, it is difficult to establish the fuzzy rule bases; (2) dynamic characteristics of the fuzzy control systems, especially in transient period, cannot be easily predicted; (3) the number of rule bases increases exponentially with the number of fuzzy input variables. This will consume substantial computational time; (4) the control parameters for the FLC are not optimized for maximum performance.

To overcome the above-mentioned difficulties (1) and (2), the switching variables are adopted in this study to form inference rule bases and force the transient dynamics to first converge the switching surface before reaching the desired states. This control technique is named "fuzzy sliding-mode control (FSMC)." As to tackle difficulty (3), another approach called regionwise linear fuzzy logic control (RLFLC) [21] is applied to reduce the number of fuzzy if–then rules. Finally, aiming for maximizing FLC performance, genetic algorithm (GA) and fuzzy neural network control (FNNC) are applied in this study to conduct off and on-line adaptations, respectively, to search for optimal control parameters. The GA [22] is a tuning/learning algorithm, which is elemented by parametrizing and encoding the control tuning parameters into binary strings in order to search for the optima. To facilitate the computation, a fitness function is defined such that the GA can search for the optimal parameters via correct directions and then

keep the evolving states on the user-defined switching surface. On the other hand, the fuzzy neural network control (FNNC) [23–36] is basically a FLC embedded in the framework of back-propagation, which combines the capability of fuzzy reasoning to handle uncertain information and that of artificial neural networks to learn from real processes in order to achieve the desired control goal.

This paper is organized as follows. In Section 2, a continuous model of the axially moving string is established. In Section 3, the sliding-mode controller is synthesized to perform vibration suppression outside the boundary layer. In Section 4, the fuzzy sliding-mode controller assisted with genetic algorithm is proposed to generate finite control effort in order to annihilate transverse vibration inside the boundary layer. In Section 5, the fuzzy neural network controller is designed to conduct on-line tuning of control parameters inside the boundary layer for a robust control performance. In Section 6, simulations are conducted to validate the effectiveness of the controllers. In Section 7, discussions are given for a better understanding of the performance of the controllers designed. In Section 8, conclusions are presented.

2. Mathematical model

The physical model of an axially moving string-like system is depicted in Fig. 1, where an axially moving string is supported at both ends by two frictionless pulleys in a constant translating speed c. An initial tension T is applied to the moving string system through the pulleys. The spatial length between the two pulleys is l. The parametric control input is realized by the variation of the string tension, denoted by $\Delta T(t)$. Neglecting the effect of the bending rigidity EI and axial vibration, the mathematical model of the system can be captured by [37]

$$\rho V_{tt}(x,\ t) + 2\rho c V_{xt}(x,\ t) + \rho c^2 V_{xx}(x,\ t) - (T + \Delta T(t)) V_{xx}(x,\ t) = 0 \tag{1}$$

subjected to the boundary conditions

$$V(0,\ t) = V(l,\ t) = 0; \quad V_t(0,\ t) = V_t(l,\ t) = 0, \tag{2}$$

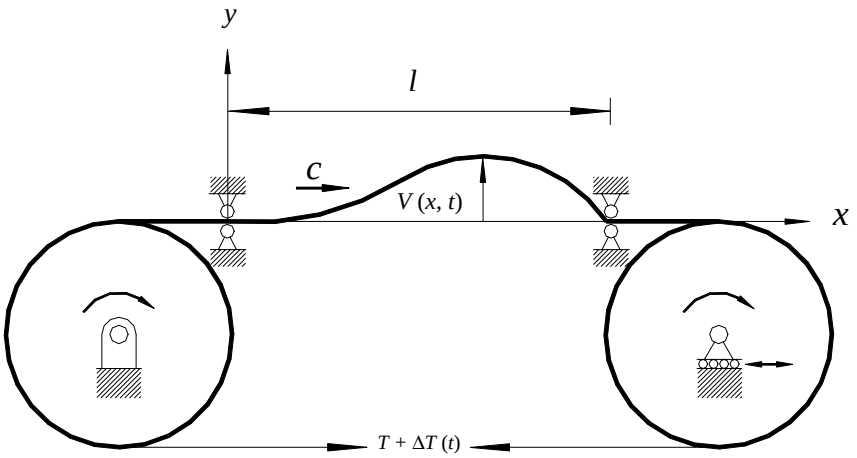

Fig. 1. Schematic of the axially moving string system.

where $V(x,\ t)$ represents the transverse displacement of string, ρ is the mass per unit length, and the subscripts denote temporal or spatial differentiations. Note that the term "$2\rho c V_{xt}(x,\ t)$" arises from gyroscopic effect. With liberty to vary $\Delta T(t)$, the transverse vibration of the string is expected to be suppressed via the control schemes designed later to regulate $\Delta T(t)$. Since the tension variation $\Delta T(t)$ originally plays the role of the system parameter in governing equation (1), the mechanism of the control to be forged can be categorized as one of "parametric controls" [15–17]. For the system prescribed in Eq. (1), the total energy of this system can be expressed as

$$E(t) = \frac{1}{2}\int_0^l \rho(V_t + cV_x)^2 \,\mathrm{d}x + \frac{T}{2}\int_0^l V_x^2 \,\mathrm{d}x. \tag{3}$$

Note in Eq. (3) that $(V_t + cV_x)$ is the combined velocity of the string in axial and transverse directions. The first and second integration terms in Eq. (3) correspond to the kinetic and potential energies, respectively.

3. Sliding-mode control design

A sliding-mode controller (SMC) is synthesized in this section in order to effectively suppress the transverse vibration of the axially moving string governed by Eq. (1). The SMC is one of the powerful control design schemes, which can be applied to either linear or non-linear systems [18]. It allows designers to force the system dynamics to first converge to the vicinity of the switching surface and then reach the origin inside the vicinity of the switching surface. The well-known Lyapunov stability analysis method is employed to ensure the stability of the controlled system. The most important elements of applying this method lie in a suitable selection of the Lyapunov functional and the effective construction of control input via Lyapunov stability analysis. For the present study, an energy-like function is first chosen as the Lyapunov function in the form of

$$\tilde{E}(t) = \frac{1}{2}\int_0^l \rho s^2 \,\mathrm{d}x + \frac{T}{2}\int_0^l V_x^2 \,\mathrm{d}x, \tag{4}$$

where $s = hV + V_t + cV_x,\ h > 0$. It can be easily seen that as the control target is set to be $\tilde{E}(t) = 0$, it is equivalent that "$s = 0$" is reached, yielding no transverse vibration for the string. It can also be shown that the energy in Eq. (4) complies with the following theorem as related to the real system energy $E(t)$ in Eq. (3).

Theorem 1. *Given the system energy function in Eq.* (3) *and Lyapunov functional in Eq.* (4), *there exist* $C_1,\ C_1 \in R$ *such that*

$$C_1 E(t) \leqslant \tilde{E}(t) \leqslant C_2 E(t). \tag{5}$$

Proof. See the appendix.

With the Lyapunov functional defined in Eq. (4), the sliding-mode control input, denoted by u_{SMC}, is next derived to reach $\dot{\tilde{E}}(t) < 0$ in order to guarantee the stability of the controlled system.

This control design process starts with the computation of $\dot{\tilde{E}}(t)$, the differentiation of the chosen energy-like Lyapunov function (4) with respect to time. Moving the differentiation inside the integrand in Eq. (4), employing the chain rule

$$\frac{\mathrm{d}}{\mathrm{d}t} = \frac{\partial}{\partial t} + c\frac{\partial}{\partial x} \tag{6}$$

and incorporating the governing equations (1) and its boundary conditions, the time-differentiation of Lyapunov functional in Eq. (4) results in

$$\dot{\tilde{E}}(t) = \int_0^l \rho s(hV_t + chV_x + V_{tt} + 2cV_{xt} + c^2V_{xx})\,\mathrm{d}x + T\int_0^l V_x(V_{xt} + cV_{xx})\,\mathrm{d}x. \tag{7}$$

Re-arrange the above equation,

$$\dot{\tilde{E}}(t) = \int_0^l \underline{s}[h\rho(V_t + cV_x) + (\underline{T} + \Delta T)\underline{V_{xx}}]\,\mathrm{d}x + T\int_0^l V_x(V_{xt} + cV_{xx})\,\mathrm{d}x. \tag{8}$$

Performing integration by parts on the underlined integrand term in Eq. (7) with incorporation of the boundary conditions (2) yields

$$\begin{aligned} T\int_0^l sV_{xx}\,\mathrm{d}x &= T\int_0^l (hV + V_t + cV_x)V_{xx}\,\mathrm{d}x \\ &= T(hV + V_t + cV_x)V_x|_0^l - T\int_0^l (hV_x + V_{xt} + cV_{xx})V_x\,\mathrm{d}x \\ &= TcV_x^2|_0^l - T\int_0^l (hV_x + V_{xt} + cV_{xx})V_x\,\mathrm{d}x. \end{aligned} \tag{9}$$

Substitution of the above Eq. (9) into Eq. (7) renders

$$\begin{aligned} \dot{\tilde{E}}(t) &= \int_0^l s[h\rho(V_t + cV_x) + \Delta TV_{xx}]\,\mathrm{d}x + TcV_x^2|_{x=l} - TcV_x^2|_{x=0} - T\int_0^l hV_x^2\,\mathrm{d}x \\ &= \Delta T\int_0^l sV_{xx}\,\mathrm{d}x + h\rho\int_0^l s(V_t + cV_x)\,\mathrm{d}x + TcV_x^2|_{x=l} - TcV_x^2|_{x=0} - T\int_0^l hV_x^2\,\mathrm{d}x. \end{aligned} \tag{10}$$

Now a suitable u_{SMC} can be designed as follows to satisfy the condition $\dot{\tilde{E}}(t) \leqslant 0$,

$$u_{SMC}(t) = \Delta T = -\left\{\frac{R_1\left|\int_0^l s(V_t + cV_x)\,\mathrm{d}x\right| + R_2V_x^2|_{x=l}}{\left|\int_0^l sV_{xx}\,\mathrm{d}x\right|}\right\} sgn\left(\int_0^l sV_{xx}\,\mathrm{d}x\right), \tag{11}$$

where R_1 and R_2 are positive constants to be determined for a target convergence speed. The essence of u_{SMC} presented in Eq. (11) resides in two key points: (i) the switching function is chosen as

$$S(t) = \int_0^l sV_{xx}\,\mathrm{d}x \tag{12}$$

and (ii) R_1 and R_2 must be determined such that $R_1 \geqslant h\rho, \quad R_2 \geqslant Tc$ in order to guarantee the stability of the controlled system. The proof is given in the following.

Theorem 2. *Given the designed effort* ΔT *as expressed in Eq.* (11) *for system* (1), *and* $\{R_1, R_2\}$ *determined with satisfaction of* $\{R_1 \geqslant h\rho, R_2 \geqslant Tc\}$, *the controlled system is exponentially stable about the origin* (*corresponding to* $\tilde{E}(t) = 0$, *i.e., no transverse vibrations*).

Proof. To show there exists a positive constant β such that

$$\dot{\tilde{E}}(t) \leqslant -\beta \tilde{E}(t) \tag{13}$$

sufficient to say that the origin with $\tilde{E}(t) = 0$ is exponentially stable. Substitution of u_{SMC} given in Eq. (11) into $\dot{\tilde{E}}(t)$ in Eq. (10) yields

$$\begin{aligned}\dot{\tilde{E}}(t) \leqslant & -(R_1 - h\rho)\left|\int_0^l (hV + V_t + cV_x)(V_t + cV_x)\,\mathrm{d}x\right| \\ & -(R_2 - Tc)V_x^2|_{x=l} - TcV_x^2|_{x=0} - hT\int_0^l V_x^2\,\mathrm{d}x \\ \leqslant & -(R_1 - h\rho)\left|\int_0^l (s^2 - shV)\,\mathrm{d}x\right| - hT\int_0^l V_x^2\,\mathrm{d}x \end{aligned} \tag{14}$$

by using the definition of s and design condition $R_2 \geqslant Tc$. Having applied the well-known triangular inequality

$$|ab| \leqslant \frac{1}{2}\left(\delta^2 a^2 + \frac{b^2}{\delta^2}\right), \tag{15}$$

where δ is a positive constant, Eq. (14) becomes

$$\begin{aligned}\dot{\tilde{E}}(t) \leqslant & -(R_1 - h\rho)\int_0^l s^2\,\mathrm{d}x + \frac{(R_1 - h\rho)h}{2}\int_0^l \left(\delta^2 s^2 + \frac{V^2}{\delta^2}\right)\mathrm{d}x - hT\int_0^l V_x^2\,\mathrm{d}x \\ = & -\left[(R_1 - h\rho) - \frac{(R - h\rho)h\delta^2}{2}\right]\int_0^l s^2\,\mathrm{d}x + \frac{(R_1 - h\rho)}{2\delta^2}\int_0^l V^2\,\mathrm{d}x - hT\int_0^l V_x^2\,\mathrm{d}x. \end{aligned} \tag{16}$$

For a continuous $V(x, t)$ and $V(0, t) = V(l, t) = 0$, based on Poincaré inequality, there exists a positive constant $\hat{\eta} > 0$ such that

$$\int_0^l V^2\,\mathrm{d}x \leqslant \hat{\eta}\int_0^l V_x^2\,\mathrm{d}x. \tag{17}$$

Incorporating Eq. (17) into Eq. (16),

$$\begin{aligned}\dot{\tilde{E}}(t) \leqslant & -\left[(R - h\rho) - \frac{(R - h\rho)h\delta^2}{2}\right]\int_0^l s^2\,\mathrm{d}x + \frac{(R - h\rho)h\hat{\eta}}{2\delta^2}\int_0^l V_x^2\,\mathrm{d}x - hT\int_0^l V_x^2\,\mathrm{d}x \\ = & -\frac{(R - h\rho)}{\rho}\left[1 - \frac{h\delta^2}{2}\right]\int_0^l \rho s^2\,\mathrm{d}x - h\left[1 - \frac{(R - h\rho)\hat{\eta}}{2\delta^2 T}\right]\int_0^l TV_x^2\,\mathrm{d}x. \end{aligned} \tag{18}$$

Let δ be chosen such that

$$\sqrt{\frac{(R-h\rho)\hat{\eta}}{2T}}<\delta<\sqrt{\frac{2}{h}}.$$

On the other hand, define

$$A_1=\frac{(R-h\rho)}{\rho}\left[1-\frac{h\delta^2}{2}\right],\quad A_2=h\left[1-\frac{(R-h\rho)\hat{\eta}}{2T\delta^2}\right].$$

Eq. (18) becomes

$$\begin{aligned}\dot{\tilde{E}}(t)&\leqslant -A_1\int_0^l \rho s^2\,\mathrm{d}x-A_2\int_0^l TV_x^2\,\mathrm{d}x\\&\leqslant -2\min\{A_1,A_2\}\left(\frac{1}{2}\int_0^l \rho s^2\,\mathrm{d}x-\frac{T}{2}\int_0^l V_x^2\,\mathrm{d}x\right)\\&\leqslant -\beta\tilde{E}(t)\end{aligned}$$

where $\beta=2\min\{A_1,\,A_2\}$. □

It can be seen from Eq. (11) that with the control input u_{SMC} discontinuous and even non-analytic at the switching surface, "$S=0$," large control effort would be generated as the states approach the vicinity of $S=0$, i.e., as the transverse vibration becomes smaller. To solve this problem, a boundary layer specified by "$|S|\leqslant S_B$" is defined such that as the states approach inside this layer, the control effort is switched from the control input u_{SMC} designed above in Eq. (11) to alternative control schemes: (i) fuzzy sliding-mode control (FSMC) or (ii) fuzzy neural network control (FNNC), in order to avoid the aforementioned non-analyticity at $S=0$. The designs of FSMC and FNNC are stated in Sections 4 and 5, respectively.

4. Design of the fuzzy sliding-mode control FSMC

To avoid the non-analyticity of the SMC near $S=0$ proposed in the last section, an hybrid control law is proposed as follows:

$$\Delta T=(1-\alpha)u_{FSMC}+\alpha u_{SMC},\tag{19}$$

where α is defined as

$$\alpha=\begin{cases}1 & \text{for}|S(t)|>S_B,\\0 & \text{for}|S(t)|\leqslant S_B.\end{cases}\tag{19a}$$

Note that in Eq. (19) u_{SMC} is the control derived in Section 3, and u_{FSMC} would be designed in this section based on the scheme of FSMC plus GA tuning technique to avoid large control effort near $S=0$. S_B in Eq. (19a) is a small positive number specifying the thickness of the boundary layer, "$|S|\leqslant S_B$." At the boundary, i.e., "$|S|=S_B$," u_{SMC} and u_{FSMC} are switched. With the hybrid control law (19) applied, at the initial evolution stage of the controlled system, i.e., as the states

are away from the boundary layer, the second term in the hybrid control law, u_{SMC}, is activated, while inside the boundary layer, the first term in hybrid control law, u_{FSMC}, is activated. The aforementioned switching mechanism provides the means to force a fast convergence of the transient dynamics via the large control effort generated by the SMC proposed in Eq. (11) outside the boundary layer, and then perform precision control via the fine-tuned effort generated by the intelligent FSMC inside the boundary layer, the mechanism of which is presented as follows.

4.1. Design of fuzzy sliding mode control

To initialize FSMC design, the switching function $S(t)$ given in Eq. (12) and its derivative are adopted to establish the fuzzy logic rules. For simplicity of computation, the derivative of switching function is considered available by a discrete approximation of

$$\dot{S}(KT) = \frac{1}{T}[S[KT - S(K-1)T], \tag{20}$$

where K is the number of sampling iteration and T is the sampling period. In order to accommodate various model characterisitics for a better control, the input functions for FSMC, S and $\dot{S}$, are multiplied by scaling factors G_S and G_{CS}, respectively. These factors are mainly used to equip the designers with the capability of adjusting control gains before S and $\dot{S}$ taken as inputs for fuzzy membership functions. The scalings give

$$\tilde{S} = S(t)G_S, \quad \dot{\tilde{S}} = \dot{S}(t)G_{CS}. \tag{21}$$

Then $\tilde{S}$ and $\dot{\tilde{S}}$ become the actual inputs for ensuing the fuzzy mechanism. The associated fuzzy sets are determined as follows:

N : negative, Z : Zero, P : positive,
NH : negative huge, NB : negative big, NM : negative medium,
NS : negative small, ZE : zero, PS : positive small,
PM : positive medium, PB : positive big, PH : positive huge.

The membership functions for the inputs $\tilde{S}$, $\dot{\tilde{S}}$ and outputs $u_{FSMC} = \Delta T$ are defined and illustrated in Fig. 2. It is seen from this figure that only five fuzzy subsets, NB, NM, Z, PM, PB, are defined for $\tilde{S}$ and $\dot{\tilde{S}}$, which require subsequently 25 fuzzy rules to accomplish the fuzzy control design. The resulting fuzzy sliding mode inference rules are shown in Table 1, where $u_{FSMC} = \Delta T$ is the fuzzy mapped function of $\tilde{S}$ and $\dot{\tilde{S}}$. Note that the essence of rules in Table 1 originates from the concept of the conventional feedback control in which u_{FSMC} plays the role of a negative feedback. Even though with the linear memberships shown in Fig. 2, the input/output relation of the fuzzy controller would not be linear with scalings $\{G_S, G_{CS}, G_R\}$ updated via Genetic Algorithm introduced in Section 4.3 to search for better memberships. Note also that by imposing the upper/lower bounds on the membership function of $u_{FSMC} = \Delta T$, one is able to realize actual saturation of control effort, which is often difficult for many control designs. (Fig. 3)

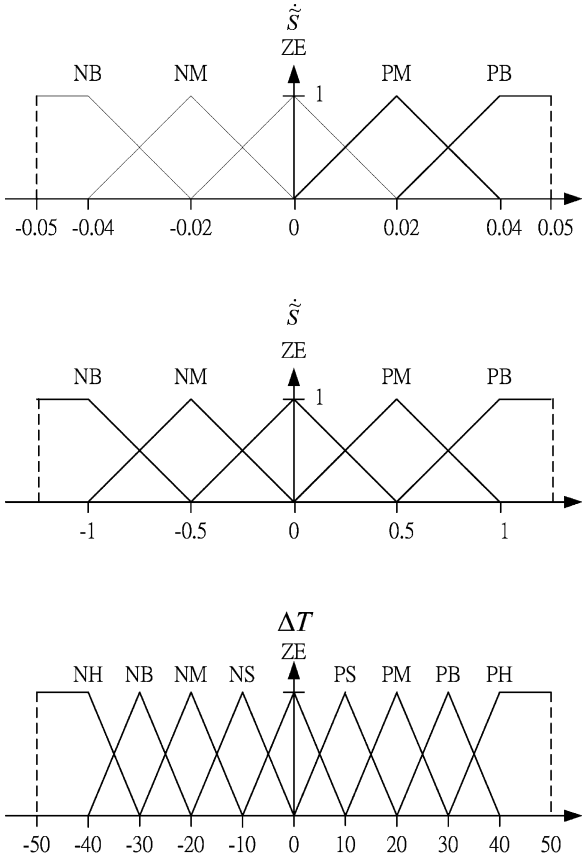

Fig. 2. The membership functions for the fuzzy sets corresponding to $\tilde{S}$, $\dot{\tilde{S}}$ and ΔT.

Table 1
Fuzzy logic linguistic rules for fuzzy sliding-mode control

ΔT	$\dot{\tilde{S}}$					
		NB	NM	Z	PM	PB
$\tilde{S}$	NB	PH	PB	PM	PS	ZE
	NM	PB	PM	PS	ZE	NS
	Z	PM	PS	ZE	NS	NM
	PM	PS	ZE	NS	NM	NB
	PB	ZE	NS	NM	NB	NH

4.2. Design of region-wise linear fuzzy logic control

As the number of input variables for fuzzy control increases, the number of fuzzy if–then rules increases exponentially; consequently, this induces a great deal of computation burden to determine fuzzy control output. In order to minimize computation load, the technique RLFLC

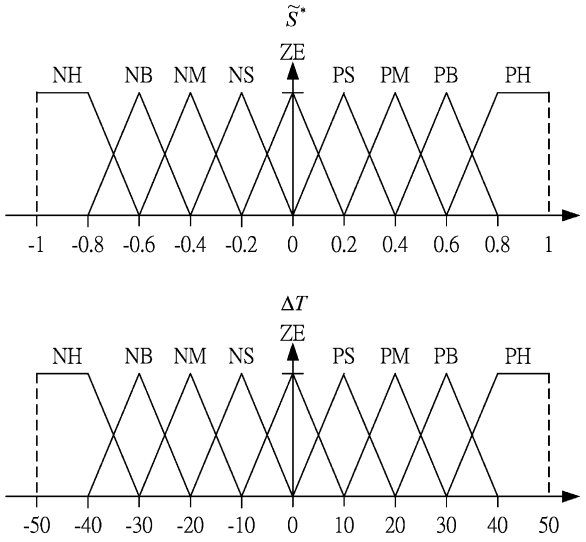

Fig. 3. Membership functions of $\tilde{S}^*$ and ΔT for RLFLC.

Table 2
Tabulated relationships between S^*, S and $\dot{S}$

ΔT	$\dot{S}$					
		NB	NM	Z	PM	PB
S	NB	NH	NB	NM	NS	ZE
	NM	NB	NM	NS	ZE	NS
	Z	NM	NS	ZE	PS	PM
	PM	NS	ZE	PS	PM	PB
	PB	ZE	PS	PM	PB	PH

[21] is applied herein to FSMC. For implementing the regionwise technique, a region-wise function $\tilde{S}^*$ is first defined by

$$S^* = S + \dot{S}, \tag{22}$$

$$\tilde{S}^* = G_R S^*, \tag{23}$$

where it is seen that to accommodate various dynamic characteristics the regionwise functions S^* are multiplied by scaling factor G_R . Table 2 lists the fuzzy relationship among S^*, S and $\dot{S}$ and reflecting Eq. (22), where the fuzzy variable S^* is defined as the composition operation of S and $\dot{S}$ in a fuzzy sense. The information revealed in both Tables 1 and 2 makes possible the derivation of the fuzzy relationship between ΔT and $\tilde{S}^*$ which is listed in Table 3. The variable $\tilde{S}^*$ is now considered the new sole fuzzy variable to synthesize fuzzy control output. Compared to the original scheme of FSMC, this method of RLFLC reduces the number of fuzzy variables from two ($\tilde{S}$ and $\dot{\tilde{S}}$) to one ($\tilde{S}^*$); as a result, the number of fuzzy linguistic rules decreases greatly. Note,

Table 3
Fuzzy logic linguistic rules for RLFLC

$\tilde{S}^*$	PH	PB	PM	PS	ZE	NS	NM	NB	NH
ΔT	NH	NB	NM	NS	ZE	PS	PM	PB	PH

however, that since the proposed RLFLC only simplifies computation procedure, the dynamic characteristics of the RLFLC are not different from those of FSMC in nature.

4.3. Genetic algorithm (GA) for scaling factor determination

The scaling factors G_s, G_{CS} in Eq. (21) and G_R in Eq. (23) allow designers to perform control gain-tunings through re-shaping of membership functions. It is expected to result in a better performance in terms of overshoot, response time, etc. The genetic algorithm (GA) is a digital numerical algorithm [22] used to search for optimum values of prescribed scalings via minimizing a pre-defined fitness function through a binary searching mechanism. The fitness function for the present study is chosen as

$$F = \sum_{t=t_0}^{t_f} \frac{1}{J + 0.1}, \tag{24}$$

where the objective function J is the discrete sum of displacement at the middle point of the string times the sampling time, i.e.,

$$J = \sum \left| V\left(\frac{l}{2}, \ t\right) \Delta t \right|, \tag{25}$$

where Δt is the sampling time. It is seen from Eq. (24) that the fitness F would be maximized by GA through minimizing the objective function J, i.e., resulting in minimizing the transverse vibration of the string. Note that for the present study optimal values of G_S , G_{CS} and G_R would be obtained off-line through an optimization process. This process demands a high accuracy of mathematical model to ensure the effectiveness of FSMC control plus GA; otherwise, satisfactory transverse vibration suppression cannot be ensured for a real string. To avoid this drawback of GA, the method of fuzzy neural network control (FNNC) is considered in the ensuing section to synthesize an on-line learning controller, u_{FNNC}, in place of u_{FSMC} in Eq. (19). The adapted neural network of FNNC provides the capability of searching for the optimum control parameters based on realistic input/output data, which does not need a precise mathematical model to function.

5. Design of the FNNC

Design of a FNNC controller, u_{FNNC}, is performed herein in two steps: (i) structure construction of FNNC, and (ii) synthesis of updating laws for FNNC.

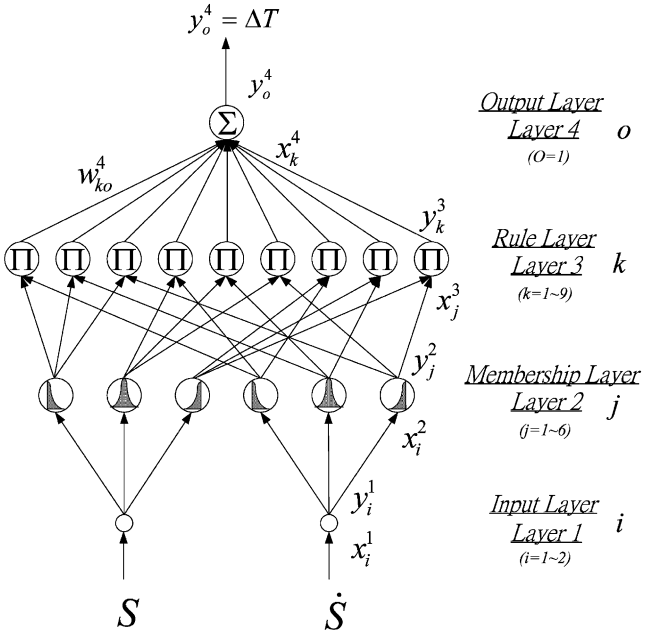

Fig. 4. Structure of the four-layer FNNC.

5.1. Structure of fuzzy neural network

A general four-layer FNNC structure shown in Fig. 4 is adopted to implement the proposed FNNC controller, which consists of the input (i layer), membership (j layer), rule (k layer), and output (o layer) layers. The switching function signal in Eq. (12) and its derivative computed by Eq. (20), S and $\dot{S}$, respectively, are chosen as two inputs to the FNNC mechanism. The output of the FNNC would be used for realizing the actuation of string tension inside the boundary layer, i.e., u_{FNNC}, in place of u_{FSMC} in Eq. (19). Two neurons in the input layer accept crisp values of S and $\dot{S}$. Those in the membership layer act as membership functions. Moreover, each neuron in the rule layer reflects a fuzzy rule base. The signal propagation in the FNNC structure and the basic function of each layer are elaborated below.

5.1.1. Layer 1 (input layer)

For each neuron i in this layer, the net input and the net output are related by

$$net_i^1 = x_i^1, \quad y_i^1 = f_i^1(net_i^1) = net_i^1, \qquad i = 1, \ 2, \tag{26}$$

where x_i^1 represents the ith input to the neuron of layer 1.

5.1.2. Layer 2 (membership layer)

In this layer, each neuron plays the role of a membership function. The Gaussian function is adopted as the membership function.

For the jth neuron,

$$net_j^2 = -\frac{(x_i^2 - m_{ij})^2}{(\sigma_{ij})^2},$$

$$y_j^2 = f_j^2(net_j^2) = \exp(net_j^2), \quad i = 1,2, \ \ j = 1-6, \tag{27}$$

where m_{ij} and σ_{ij} are, respectively, the mean and the standard deviations of the Gaussian function for the membership in the jth neuron, which takes the ith linguistic variable x_i^2 as the input. Note that the objective of layer 2 are to form the membership functions for incorporating the fuzzy logics in the structure of neural network, and then updating m_{ij} and σ_{ij} to find the optimum shapes of memberships for a minimum error defined later. Unlike the traditional back-propagation scheme, the weights between layers 1 and 2 are set as unities, leaving adaptation responsibility to varying m_i's and σ_{ij}'s. As a result, in Fig. 4, the weights between layers 1 and 2 are not denoted.

5.1.3. Layer 3 (rule layer)

Each neuron k in this layer is denoted by $\prod$, which multiplies the incoming signal with weightings and outputs the resulting product. For the kth rule neuron,

$$net_k^3 = \prod_j w_{jk}^3 x_j^3, \ \ y_k^3 = f_k^3(net_k^3) = net_k^3, \quad j = 1-6, \ \ k = 1-9, \tag{28}$$

where x_j^3 represents the jth input to the neuron of layer 3. The weights between layers 2 and 3 are also set to be unities, leaving the remaining adaptation capability of this FNNC scheme to be performed in layer four.

5.1.4. Layer 4 (output layer)

The single neuron o in this layer is labelled by $\sum$, which computes the overall output by summing all incoming signals by

$$net_0^4 = \sum_k w_{ko}^4 x_k^4, \ \ y_o^4 = f_o^4(net_o^4) = net_o^4, \ \ o = 1, \tag{29}$$

where the link weights w_{ko}^4's are the output action strength of the oth output associated with the kth rule; x_k^4 represents the kth input to the neuron of layer 4, y_o^4 is the output of the neural network. In practice, y_o^4 is realized by the actuation of the tension force; i.e., $y_o^4 = u_{FNNC} = \Delta T$.

5.2. Updating laws

Another key design part for FNNC other than neural network structure presented in the last subsection is to obtain learning algorithms for each updating parameter, which can be accomplished by computing the derivatives of a defined error function with respect to the updating parameters through the established neural network. This is done by means of the chain rule, and the method is generally referred to as the back-propagation learning because the updating laws are calculated in the direction opposite to the flow of real data processing [27]. The computation of the updating laws starts with defining the error function as $S\dot{S}$ in order to

maximize convergence speed to approach $S=0$. The expression of $S\dot{S}$ is next derived to realize updating computation, which is achieved based on the definition of switching function S in Eq. (12) and its time-derivative, yielding

$$S\dot{S} = S\int_0^l \left(hV_t|hcV_x + \frac{T}{\rho}V_{xx}\right)V_{xx}\,\mathrm{d}x + \frac{1}{\rho}\Delta T(t)S\int_0^l V_{xx}^2\,\mathrm{d}x + S\int_0^l (hV + V_t + cV_x)(V_{xxt} + cV_{xxx})\,\mathrm{d}x. \tag{30}$$

With the explicit expression of the error function (30) in hand, the updating laws for each layer is derived as follows for FNNC to function.

5.2.1. Layer 4

Based on the basic concept of gradient descent, the weights in the output layer are updated as follows:

$$\Delta w_{ko}^4 = -\eta\frac{\partial S\dot{S}}{\partial \Delta T}\frac{\partial \Delta T}{\partial w_{ko}^4} = -\eta\left(\frac{S}{\rho}\int_0^l V_{xx}^2\,\mathrm{d}x\right)x_k^4 = -\left(\frac{\eta}{\rho}\right)S\int_0^l V_{xx}^2\,\mathrm{d}x x_k^4 = -\gamma S\int_0^l V_{xx}^2\,\mathrm{d}x x_k^4, \tag{31}$$

where η is a positive constant, and $\gamma = (\eta/\rho)$ is the learning-rate parameter of the weights to be designed. The weights of the output layer are updated according to the following equation:

$$w_{ko}^4(N+1) = w_{ko}^4(N) + \Delta w_{ko}^4, \tag{32}$$

where N denotes the sampling iteration number. The initial values of weights are set to be uniform over the output space of layer 3 for simplicity.

5.2.2. Layer 3

In this layer since the weights in the rule layer are set to be unities, only the approximated error term needs to be calculated by

$$\delta_k^3 \triangleq \left[-\frac{\partial S\dot{S}}{\partial \Delta T}\frac{\partial \Delta T}{\partial net_o^4}\frac{\partial net_o^4}{\partial y_k^3}\frac{\partial y_k^3}{\partial net_k^3}\right] = -\left(\frac{s}{\rho}\int_0^l V_{xx}^2\,\mathrm{d}x\right)w_{ko}^4. \tag{33}$$

5.2.3. Layer 2

As multiplications are conducted in the membership layer, the error term is computed as follows:

$$\delta_k^2 \triangleq \left[-\frac{\partial S\dot{S}}{\partial \Delta T}\frac{\partial \Delta T}{\partial net_o^4}\frac{\partial net_o^4}{\partial y_k^3}\frac{\partial y_k^3}{\partial net_k^3}\right]\left[\frac{\partial net_k^3}{\partial y_j^2}\frac{\partial y_j^2}{\partial net_j^2}\right] = \sum_k \delta_k^3 y_k^3. \tag{34}$$

The update laws for m_{ij}'s and σ_{ij}'s are obtained by the gradient descent search algorithm, i.e.,

$$\Delta m_{ij} = -\eta_m \frac{\partial S\dot{S}}{\partial m_{ij}} = \left[-\eta_m \frac{\partial S\dot{S}}{\partial y_j^2} \frac{\partial y_j^2}{\partial net_j^2} \frac{\partial net_j^2}{\partial m_{ij}} \right] = \eta_m \delta_j^2 \frac{2(x_i^2 - m_{ij})}{(\sigma_{ij})^2}, \tag{35}$$

$$\Delta \sigma_{ij} = -\eta_\sigma \frac{\partial S\dot{S}}{\partial \sigma_{ij}} = \left[-\eta_\sigma \frac{\partial S\dot{S}}{\partial y_j^2} \frac{\partial y_j^2}{\partial net_j^2} \frac{\partial net_j^2}{\partial \sigma_{ij}} \right] = \eta_\sigma \delta_j^2 \frac{2(x_i^2 - m_{ij})}{(\sigma_{ij})^3}, \tag{36}$$

where the factors η_m's andη_σ's are the learning-rate parameters of the means and the standard deviations for Gaussian membership functions to be designed, respectively. The means and standard deviations of the membership layer are updated as follows,

$$m_{ij}(N+1) = m_{ij}(N) + \Delta m_{ij}, \tag{37}$$

$$\sigma_{ij}(N+1) = \sigma_{ij}(N) + \Delta \sigma_{ij} \tag{38}$$

6. Numerical simulation

The numerical technique of finite difference is used herein to discretize the governing PDE (1) and simulate the response of the system. The total length of the string is discretized in N sections by equal section length Δx, while the temporal axis is discretized by Δt. The spatial integration is approximated via the trapezoidal integration method. The stability for the convergence of the finite difference criterion is [38]

$$\Delta t \leqslant \frac{\Delta x^2}{2}. \tag{39}$$

With $N = 20$ and $l = 1$ (since l is already normalized) Δ_x .and Δ_t .are chosen to be 0.05 and 0.00125, respectively, to render $\Delta t/\Delta x^2 = 0.5$, satisfying the convergence criterion (39). On the other hand, the parameters of the string-like system used are as follows. The initial tension is $T = 45$N. The saturation limit for control effort, variation of string tension is set as $\Delta T_{max} = 50$N; mass per unit length is $\rho = 1$Kg/m, string length is $l = 1$ m, translating speed is constant as. $c = 0.1$m/s Finally, the initial transverse shape of the string is assumed by $V(x, 0) = 0.05\sin(\pi x/l)$.

Fig. 5 shows the simulation results for the case in which the design of SMC is applied outside the boundary layer, while FSMC is applied inside the boundary layer without assistance of GA, where the solid curves represent the controlled case while the dotted curves represent the uncontrolled case. Figs. 5(a) and (b) show the history of displacements at middle point ($l = \frac{1}{2}$) and the first quarter point ($l = \frac{1}{4}$) of the axially moving string, respectively. In order to guarantee $\dot{\tilde{E}}(t) < 0$, the constants R_1 and R_2 in $u_{SMC}(t)$ in control law (11) are first chosen as $R_1 = 10$ and $R_2 = 10$, and the boundary layer is determined by $S_B = 0.01$. Fig. 5(c) shows the time history of total mechanical energy given by Eq. (3). Fig. 5(d) shows time history of

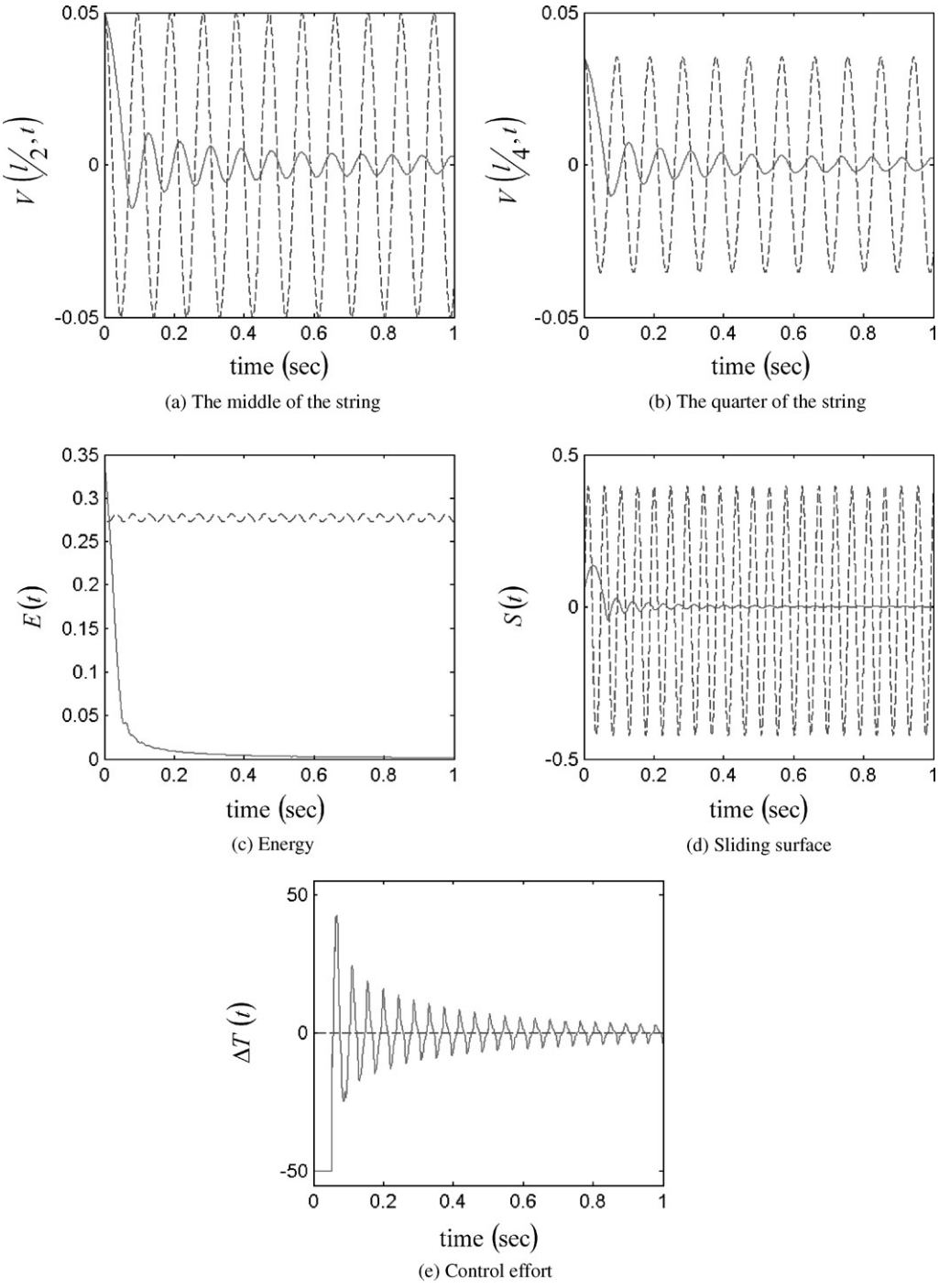

Fig. 5. Simulation results by FSMC; (a) the transverse vibration amplitude at the midpoint of the string; (b) the transverse vibration amplitude at the quarter point of the string; (c) the total energy of the controlled system, (d) switching function; (e) control effort. "…" represents the results related to uncontrolled system. "-" represents the results related to controlled system with $R_1 = 10$, $R_2 = 10$ and unity scalings.

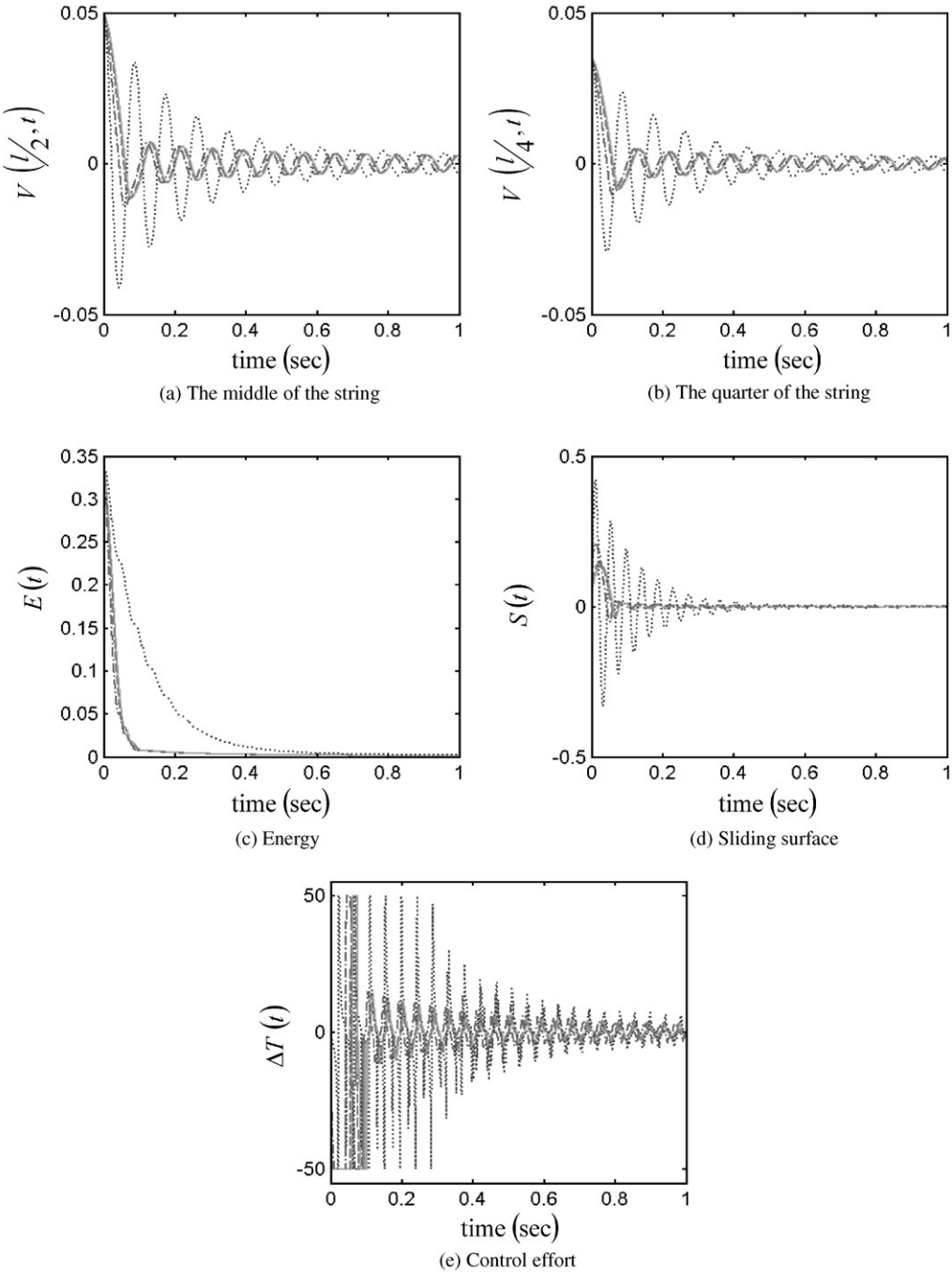

Fig. 6. Simulation results by FSMC with unity scalings and various (R_1, R_2); (a) the transverse vibration amplitude at the midpoint of the string; (b) the transverse vibration amplitude at the quarter point of the string; (c) the total energy of the controlled system, (d) switching function; (e) control effort. "…" represents the results related to the controlled system with $(R_1, R_2) = (20, 20)$. "-." represents those with $(R_1, R_2) = (20, 20)$. "–" represents those with $(R_1, R_2) = (40, 40)$, "-" represents those with largest gains $(R_1, R_2) = (100, 100)$.

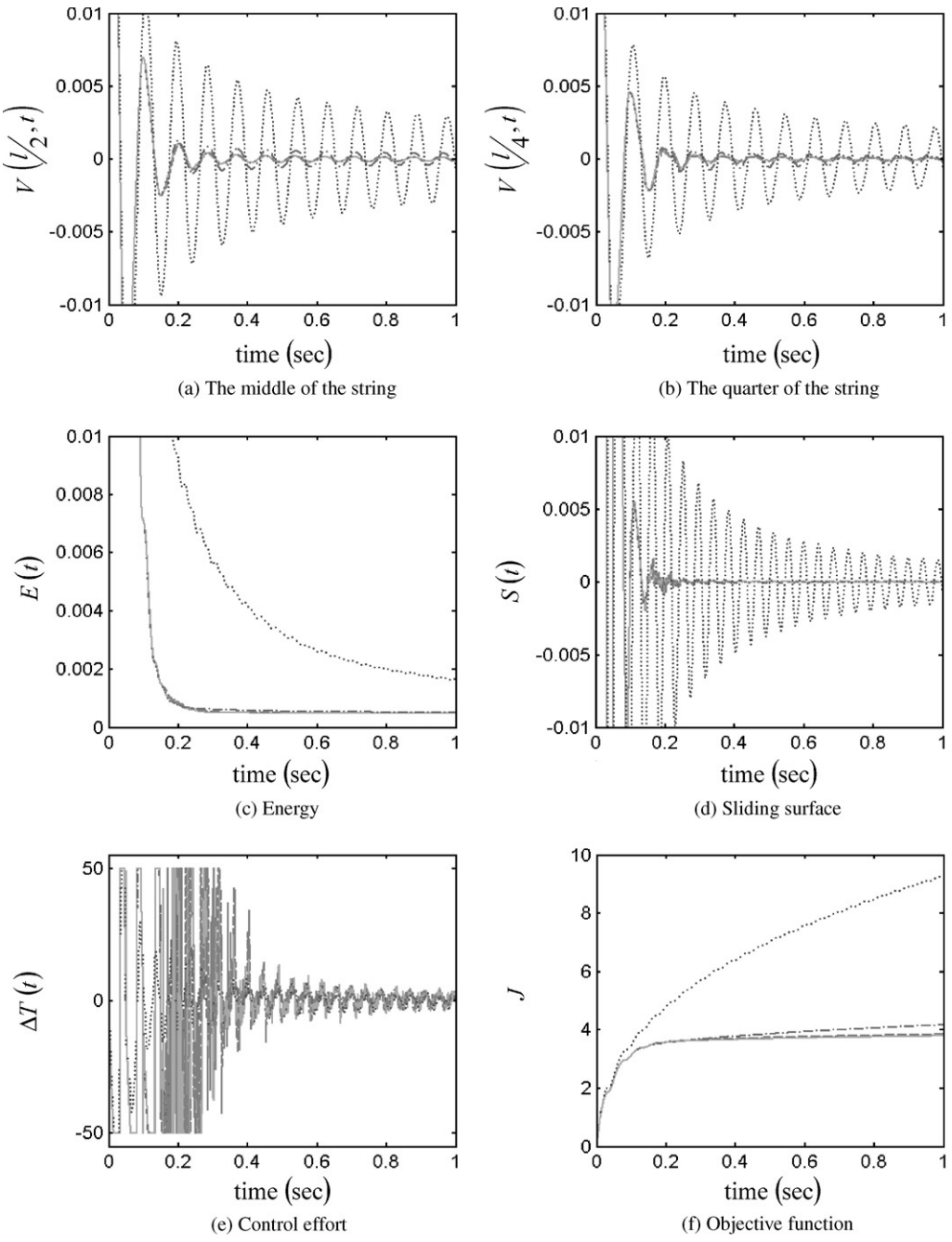

Fig. 7. Simulation results by FSMC assisted by GA with $(R_1, R_2) = (100, 100)$ and various scalings of (G_S, G_{CS}); (a) the transverse vibration amplitude at the midpoint of the string; (b) the transverse vibration amplitude at the quarter point of the string; (c) the total energy of the controlled system, (d). switching function; (e) control effort; (f) objective function. "…" represents the results related to the controlled system with $(G_S, G_{CS}) = (10, 1)$. "-." represents those controlled system with $(G_S, G_{CS}) = (80, 1)$. "–-" represents those with $(G_S, G_{CS}) = (100, 1)$. "-" represents those with the optimal gain $(G_S, G_{CS}) = (100, 10)$.

switching function $S(t)$, where it is seen that the state trajectory approaches the boundary layer $\{S < S_B = 0.01\}$ in a short period of time; then oscillates around the switching surface $S = 0$ to zero vibration after the control mechanism is switched from SMC to FSMC. Fig. 5(e) shows the corresponding control effort, where it is seen that as the states are inside the boundary layer, the control effort generated by FSMC remains finite. It is seen from Figs. 5(a) and (b), based on the comparison between controlled and uncontrolled cases that the transverse vibration of the controlled systems is successfully suppressed after the designed hybrid controller is applied.

To obtain possibly better vibration suppression at midpoint of the string, the influence of parameters R_1 and R_2 on SMC performance outside the boundary layer is explored based on related simulations shown in Figs. 6(a)–(e), where dotted, dot–dashed, dashed and solid curves represent the cases with the $(R_1, R_2) = (1, 5)$, (20 20), (40, 40) and (100, 100), respectively. It can be seen from these figures that as (R_1, R_2) increased from (1, 5) to (20, 20), the convergence speed is increased significantly, while (R_1, R_2) increased from (20, 20) to (100, 100), the convergence speed is increased in a moderate level. This reveals that with large (R_1, R_2), the convergence speed does not vary significantly outside the boundary layer, which is in fact due to the realistic saturation limitation, $\Delta T_{max} = 50$N, imposed on the control effort.

The influence of the chosen values of G_S and G_{CS} on the performance of FSMC equipped with GA technique applied inside the boundary layer is exploited next based on simulations. Figs. 7(a)–(f) show the related results where dotted, dot–dashed, dashed and solid curves represent the cases with $(G_S, G_{CS}) = (10, 1)$, (80, 1), (100, 1) and the optimum ones $(G_S, G_{CS}) = (100, 10)$, respectively. Fig. 7(f) shows the history of the objective function defined in Eq. (25). It is seen from these figures that the optimum scalings, $(G_S, G_{CS}) = (100, 10)$, obtained by the GA technique renders faster vibration suppression and smoother system response of the string as compared to those with other values of (G_S, G_{CS}) employed. This demonstrates the effectiveness of the GA technique.

Fig. 8 shows the simulated results using the design schemes of RLFLC equipped with the technique of GA where dotted, dot–dashed, dashed and solid curves represent the cases with $G_R = \{10, 50, 80\}$ and the optimum one, $G_R = 100$, respectively. It is seen from these figures that the optimum scaling $G_R = 100$ leads to faster vibration suppression and smoother system response. On the other hand, it is also seen that as compared to the simulated results of FSMC with GA shown in Fig. 7, a reduction in number of rule bases by RLFLC still renders similar general dynamic characteristics of the controlled system. This is due to the fact that RLFLC only provides a simplified computation technique of the fuzzy logic reasoning rather than changing the dynamic nature of the controllers.

Fig. 9 shows the simulated results using the FNNC scheme inside the boundary layer. Dotted curves represent the uncontrolled case while dashed and solid curves show the controlled results with the learning rate $\gamma = 0.1$ and 0.2, respectively. Other learning rates are set as $\eta_m = \eta_\sigma = 0.05$. It is seen from the figures that the larger γ is used, the faster decay of the string transverse vibration is obtained either at first quarter point or midpoint of the moving string. One can also note, as compared to the controlled responses from Figs. 8(a), (b) and 9(a), (b), respectively, that the convergence speed via FSMC with GA is faster than that via FNNC. This shows the advantage of the FSMC with GA over FNNC as the precision of the mathematical model is assured.

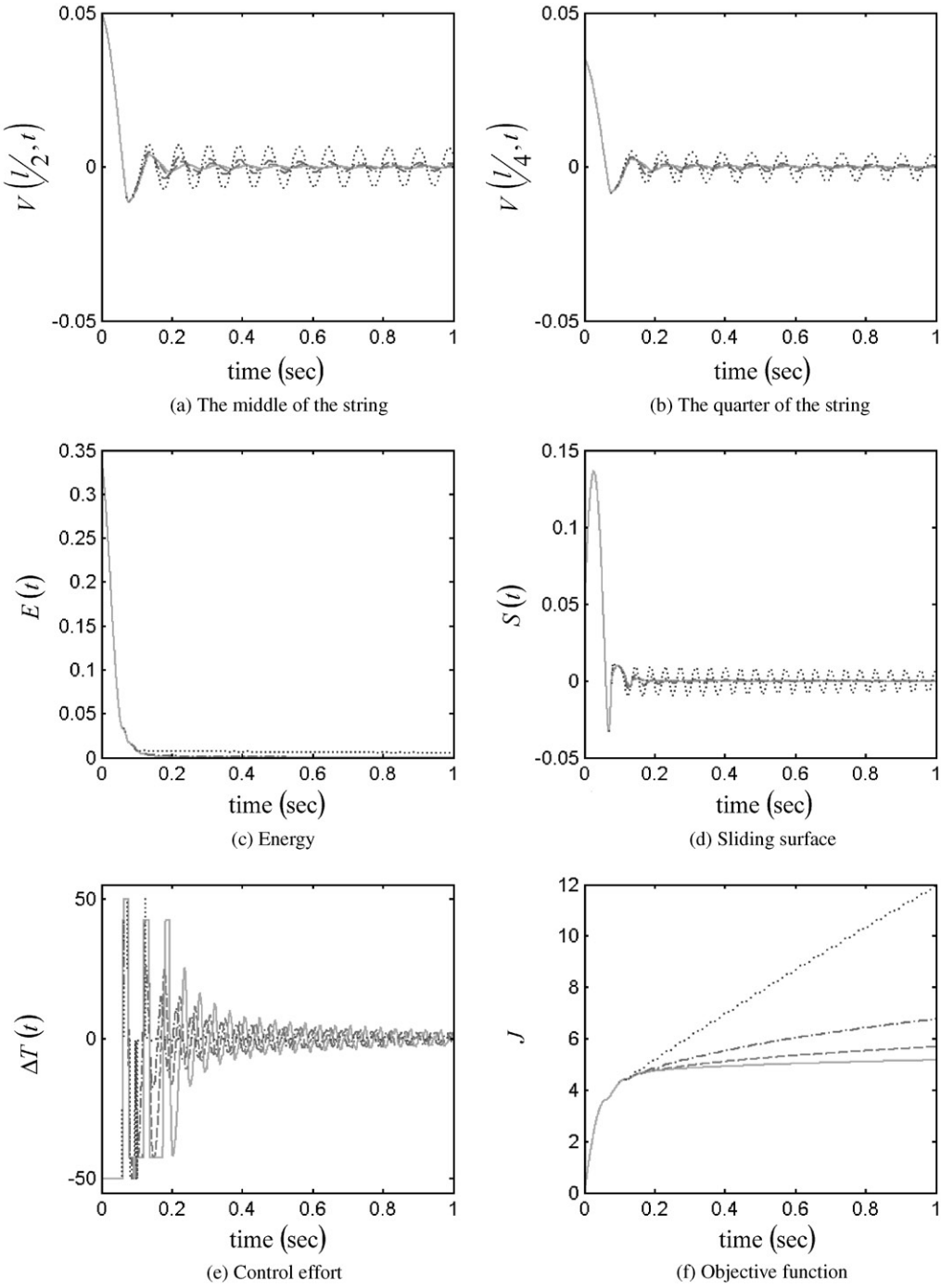

Fig. 8. Simulation results by RLFLC assisted by GA with various G_R; (a) the transverse vibration amplitude at the midpoint of the string; (b) the transverse vibration amplitude at the quarter point of the string; (c) the total energy of the controlled system, (d) switching function; (e) control effort; (f) objective function. "…" represents the results related to the controlled system with $G_R = 10$. "-." represents those the with $G_R = 50$. "–" represents those with $G_R = 80$. "-" represents those with the optimal gain G_R.

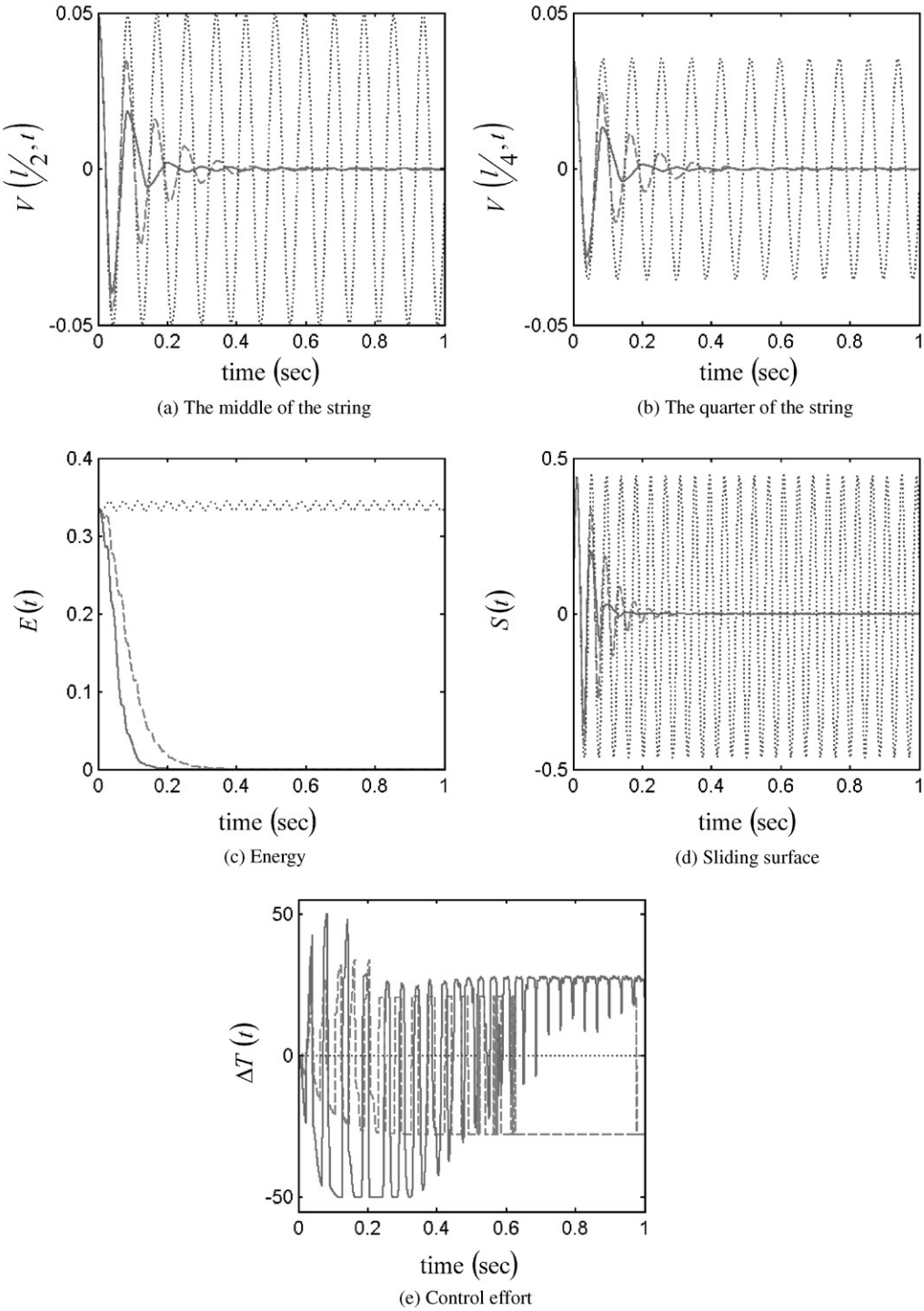

Fig. 9. Simulation results by FNNC(a) the transverse vibration amplitude at the midpoint of the string; (b) the transverse vibration amplitude at the quarter point of the string; (c) the total energy of the controlled system, (d) switching function; (e) control effort. "…" represents the results related to the uncontrolled system. "–" represents the controlled system with smaller learning rate $\gamma = 0.1$. "-" represents the controlled system with largerlearning rate $\gamma = 0.2$.

7. Discussions

Remarks related to controller performance are provided at this point.

- It was shown by simulations that the proposed hybrid controller in Eq. (19) — using sliding-mode control as the states away from the switching surface and intelligent controls as approaching the switching surface — is capable of stabilizing the systems dynamics in a fast convergent speed while avoiding large control efforts as approaching the switching surface, reducing the transverse vibration of the axially moving string in a fast and smooth fashion.
- Two different intelligent control techniques were proposed as the states are inside the boundary layer around the switching surface: (i) FSMC equipped with GA and (ii) FNNC. As mentioned in the end of Section 4, a precise dynamic model is needed for the FSMC equipped with GA to find realistically functional optimal scalings. Without sufficient confidence on the dynamic model, the FNNC should then be used instead to overcome model uncertainty even though it consumes considerable amount of computation time to search for optimal weights and parameters.

8. Conclusions

The active parametric control intended for transverse vibration suppression of an axially moving string was designed via adjustment of string tension in this study. With governing dynamic equations in the forms of partial differential equations established, a newly developed hybrid control scheme was proposed to carry out vibration suppression. The hybrid control consists of two different control strategies applied at two different stages of convergence evolution of the controlled system dynamics. The conventional sliding-mode control (SMC) was applied first outside the prescribed boundary layer around the switching surface to render a fast convergence, which was followed by activation of an intelligent control scheme — fuzzy sliding-mode control (FSMC) equipped with GA or fuzzy neural network control (FNNC) — to perform fine-tuning inside the boundary. Other than the above-mentioned control designs, to ease the computation load of fuzzy mechanism, the technique of regionwise linear fuzzy logic control (RLFLC) was also employed to assist the computation related to fuzzy control. Numerical simulations are performed to validate the effectiveness of the controls designed and to explore the influence of different control parameters on controller performance. The simulation results show that the proposed controllers are able to achieve satisfactory vibration suppression. With the precise mathematical model obtained, the FSMC equipped with GA would perform the best through an off-line process of searching for optimal scalings, while without sufficient confidence on the dynamic model, the FNNC would be a better choice to overcome model uncertainty even though it consumes considerable amount of computation time to search for optimal weights and parameters.

Acknowledgements

The authors would like to thank the to National Science Council of R.O.C. for their financial support through contracts numbered NSC 90-2212-E-033-010 and NSC 90-2212-E-033-004.

Appendix

Proof of Theorem 1. The upper bound part in Eq. (5) is shown first. The Lyapunov function (4) can be rewritten as

$$\begin{aligned}\tilde{E}(t) &= \frac{1}{2}\int_0^l \rho(hV + V_t + cV_x)^2 \,\mathrm{d}x + \frac{T}{2}\int_0^l V_x^2 \,\mathrm{d}x \\ &= \frac{1}{2}\int_0^l \rho(hV)^2 \,\mathrm{d}x + \int_0^l \rho hV(V_t + cV_x)\,\mathrm{d}x \\ &\quad + \frac{1}{2}\int_0^l \rho(V_t + cV_x)^2 \,\mathrm{d}x + \frac{T}{2}\int_0^l V_x^2 \,\mathrm{d}x. \end{aligned} \tag{A.1}$$

Incorporating inequalities (15) and (17), Eq. (A.1) becomes

$$\begin{aligned}\tilde{E}(t) &\leqslant \frac{1}{2}\int_0^l \rho c^2 \,\mathrm{d}x + \frac{\rho h^2\eta}{2}\int_0^l V_x^2 \,\mathrm{d}x + \frac{\rho h}{2}\int_0^l \left[\varepsilon^2 V^2 + \frac{(V_t + cV_x)^2}{\varepsilon^2}\right] \mathrm{d}x \\ &\quad + \frac{1}{2}\int_0^l \rho(V_t + cV_x)^2 \,\mathrm{d}x + \frac{T}{2}\int_0^l V_x^2 \,\mathrm{d}x \\ &= \frac{1}{2}\int_0^l \rho c^2 \,\mathrm{d}x + \frac{\rho h}{2}\int_0^l \varepsilon^2 V^2 \,\mathrm{d}x + \frac{1}{2}\left[1 + \frac{h}{\varepsilon^2}\right]\int_0^l \rho(V_t + cV_x)^2 \,\mathrm{d}x \\ &\quad + \frac{T}{2}\left[1 + \frac{\rho h^2\eta}{T}\right]\int_0^l V_x^2 \,\mathrm{d}x, \end{aligned} \tag{A.2}$$

where ε is an arbitrary positive constant. The Poincaré's inequality (17) is applied on Eq. (A.2), yielding

$$\begin{aligned}\tilde{E}(t) &\leqslant \frac{1}{2}\int_0^l \rho c^2 \,\mathrm{d}x + \frac{\rho h\varepsilon^2\eta}{2}\int_0^l V_x^2 \,\mathrm{d}x + \frac{1}{2}\left[1 + \frac{h}{\varepsilon^2}\right]\int_0^l \rho(V_t + cV_x)^2 \,\mathrm{d}x \\ &\quad + \frac{T}{2}\left[1 + \frac{\rho h^2\eta}{T}\right]\int_0^l V_x^2 \,\mathrm{d}x \\ &= \frac{1}{2}\int_0^l \rho c^2 \,\mathrm{d}x + \frac{1}{2}\left[1 + \frac{h}{\varepsilon^2}\right]\int_0^l \rho(V_t + cV_x)^2 \,\mathrm{d}x + \frac{T}{2}\left[1 + \frac{\rho h\eta(h + \varepsilon^2)}{T}\right]\int_0^l V_x^2 \,\mathrm{d}x \\ &\leqslant \max\left\{1 + \frac{h}{\varepsilon^2},\ 1 + \frac{\rho h\eta(h + \varepsilon^2)}{T}\right\}\left[\frac{1}{2}\int_0^l \left[c^2 + \rho(V_t + cV_x)^2\right] \mathrm{d}x + \frac{T}{2}\int_0^l V_x^2 \,\mathrm{d}x\right] \\ &= C_2 E(t). \end{aligned}$$

The lower bound part of Eq. (5) is to be shown next with the Lyapunov function (4) first rewritten as

$$\tilde{E}(t) = \frac{1}{2}\int_0^l \rho(hV + V_t + cV_x)^2 \,\mathrm{d}x + \frac{T}{2}\int_0^l V_x^2 \,\mathrm{d}x$$

$$
\begin{aligned}
&= \frac{1}{2}\int_0^l \rho(hV)^2\,\mathrm{d}x + \int_0^l \rho hV(V_t + cV_x)\,\mathrm{d}x + \frac{1}{2}\int_0^l \rho(V_t + cV_x)^2\,\mathrm{d}x + \frac{T}{2}\int_0^l V_x^2\,\mathrm{d}x \\
&\geqslant -\frac{1}{2}\int_0^l \rho c^2\,\mathrm{d}x + \int_0^l \rho hV(V_t + cV_x)\,\mathrm{d}x + \frac{1}{2}\int_0^l \rho(V_t + cV_x)^2\,\mathrm{d}x + \frac{T}{2}\int_0^l V_x^2\,\mathrm{d}x \\
&\geqslant -\frac{1}{2}\int_0^l \rho c^2\,\mathrm{d}x - \frac{\rho h}{2}\int_0^l \left[\varepsilon^2 V^2 + \frac{(V_t + cV_x)^2}{\varepsilon^2}\right]\mathrm{d}x + \frac{1}{2}\int_0^l \rho(V_t + cV_x)^2\,\mathrm{d}x \\
&\quad + \frac{T}{2}\int_0^l V_x^2\,\mathrm{d}x.
\end{aligned}
$$

Using Poincaré's inequality in Eq. (17), Eq.(A.3) becomes

$$
\begin{aligned}
\tilde{E}(t) &\geqslant -\frac{1}{2}\int_0^l \rho c^2\,\mathrm{d}x - \frac{\rho h\varepsilon^2\eta}{2}\int_0^l V_x^2\,\mathrm{d}x + \frac{1}{2}\left[1 - \frac{h}{\varepsilon^2}\right]\int_0^l \rho(V_t + cV_x)\,\mathrm{d}x + \frac{T}{2}\int_0^l V_x^2\,\mathrm{d}x \\
&= -\frac{1}{2}\int_0^l \rho c^2\,\mathrm{d}x + \frac{1}{2}\left[1 - \frac{h}{\varepsilon^2}\right]\int_0^l \rho(V_t + cV_x)\,\mathrm{d}x + \frac{T}{2}\left[1 - \frac{\rho h\varepsilon^2\eta}{2T}\right]\int_0^l V_x^2\,\mathrm{d}x. \\
&\geqslant \min\left\{-1, 1 - \frac{h}{\varepsilon^2}, 1 - \frac{\rho h\varepsilon^2\eta}{2T}\right\}\left(\frac{1}{2}\int_0^l \rho c^2\,\mathrm{d}x + \frac{1}{2}\int_0^l \rho(V_t + cV_x)\,\mathrm{d}x + \frac{T}{2}\int_0^l V_x^2\,\mathrm{d}x\right) \\
&= C_1 E(t). \qquad \square
\end{aligned}
$$

References

[1] C.D. Mote Jr., Dynamic stability of axially moving materials, Shock Vibration Digest 4 (1972) 2–11.

[2] J.A. Wickert, C.D. Mote Jr., On the energetic of axially moving continua, Journal of the Acoustic Society of America 85 (1989) 1365–1368.

[3] J.A. Wickert, C.D. Mote Jr., Classical vibration analysis of axially moving continua, American Society of Mechanical Engineers Journal of Applied Mechanics 57 (1990) 738–744.

[4] M.J. Balas, Feedback control of flexible system, IEEE Transactions on Automatic Control 23 (4) (1978) 637–679.

[5] M.J. Balas, Toward a more practical control theory for distributed parameter system, Control and Dynamics System, Vol. 18, Academic Press, New York, 1982, pp. 361–421.

[6] L. Meirovitch, H. Baruh, Control of self-adjoint distributed-parameter systems, Journal of Guidance and Control 5 (1) (1982) 60–66.

[7] A.E. Jai, A.J. Pritchard, Sensors and actuators in distributed systems, International Journal of Control 46 (1987) 1139–1153.

[8] M.J. Balas, R. Quan, R. Davidson, B. Das, Low-order control of large aerospace structures using residual mode filters, Recent Advanced in Control of Nonlinear and Distributed Parameter Systems, Robust Control and Aerospace Applications, American Society of Mechanical Engineers, New York, 1988 pp. 157–165.

[9] C.L. Lin, F.B. Hsiao, B.S. Chen, Stabilization of large structural systems under mode truncation, parameter perturbations and actuator saturation, International Journal of Systems Science 21 (8) (1990) 1423–1440.

[10] K. Nonami, J. Wang, W.M. Sampei, T. Mita, Active vibration control of a flexible rotor using H-infinity control theory, JSME International Journal, Series C 35 (3) (1992) 393–409.

[11] P.L.D. Peres, E.R. De Pieri, H. Abou-Kandil, Robust output feedback control applied to flexible structures, Proceedings of the IFAC/IFORS/IMACS Symposium on Large Scale Systems: Theory and Applications, Beijing, China, 1992, pp. 476–479.

[12] C.R. Burrows, P.S. Keogh, R. Tasaltin, Closed-loop vibration control of flexible rotors — and experimental study, Proceedings of the Institution of Mechanical Engineers, Part C. Mechanical Engineering Science 207 (1) (1995) 1–7.
[13] N.S. Khot, H. Oz, Structural-control optimization with H-2 and H-infinity norm bounds, Optimal Control Applications and Methods 18 (1997) 297–311.
[14] J.H. Chou, S.H. Chen, C.H. Chao, Robust stabilization of flexible mechanical systems under noise uncertainties and time-varying parameter perturbations, Journal of Vibration and Control 4 (2) (1998) 167–185.
[15] C.D. Rahn, C.D. Mote Jr., Parametric control of flexible systems, Journal of Vibration and Acoustics 116 (1994) 379–385.
[16] C.D. Rahn, C.D. Mote Jr., Parametric control of conservative mechanical systems, Journal of Dynamic Systems, Measurement, and Control 118 (1996) 309–314.
[17] C.D. Rahn, C.D. Mote Jr., Axial force stabilization of transverse vibration in pinned and clamped beams, Journal of Dynamic Systems, Measurement, and Control 118 (1996) 379–380.
[18] L. Slotine, Applied Nonlinear Control, Prentice-Hall, Englewood Cliffs, NJ, 1991.
[19] L.A. Zadeh, Fuzzy sets, Information and Control 8 (1965) 338–353.
[20] P.J. King, E.H. Mamdani, Application of fuzzy algorithms for control of simple dynamic plant, Proceeding IEE 121 (1974) 1585–1588.
[21] J.S. Taur, C.W. Tao, Design and analysis of region-wise linear fuzzy controllers, IEEE Transactions on Systems, Man and Cybernetics 27 (1997) 526–532.
[22] S.C. Lin, Y.Y. Chen, Design of self-learning fuzzy sliding mode controllers based in genetic algorithms, Fuzzy Sets and Systems 86 (1997) 139–153.
[23] C.C. Lee, Fuzzy logic in control systems: fuzzy logic controller—part I and part II, IEEE Transactions on Systems, Man and Cybernetics 20 (2) (1990) 404–436.
[24] R.R. Yager, D.P. Filev, Essentials of Fuzzy Modelling and Control, Wiley, New York, 1994.
[25] L.X. Wang, Adaptive Fuzzy Systems and Control: Design and Stability Analysis, Prentice-Hall, New York, 1994.
[26] S. Commuri, F.L. Lewis, Adaptive fuzzy logic control of robot manipulators, Proceedings of the IEEE, Robotics and Automation, 1996, pp. 2604–2609.
[27] T. Fukuda, T. Shibata, Theory and applications of neural networks for industrial control systems, IEEE Transactions on Industrial Electronics 39 (6) (1992) 472–489.
[28] P.S. Sastry, G. Santharam, K.P. Unnikrishnan, Memory neuron networks for identification and control of dynamical systems, IEEE Transactions on Neural Networks 5 (2) (1994) 306–319.
[29] Y. Zhang, P. Sen, G.E. Henran, An on-line trained adaptive neural controller, IEEE Control Systems Magazine 15 (5) (1995) 67–75.
[30] C.C. Ku, K.Y. Lee, Diagonal recurrent networks for dynamic systems control, IEEE Transactions on Neural Networks 6 (1) (1995) 144–156.
[31] C.T. Lin, C.S.G. Lee, Neural-network-based fuzzy logic control and decision system, IEEE Transactions on Communications 40 (12) (1991) 1320–1336.
[32] S. Horikawa, T. Furuhashi, Y. Uchikawa, On fuzzy modelling using fuzzy neural networks with the backpropagation algorithm, IEEE Transactions on Neural Networks 3 (5) (1992) 801–806.
[33] A. Ismael, B. Hussien, R.W. Mclaren, Fuzzy neural network implementation of self tuning PID control, Proceedings of the IEEE International Symposium on Intelligent Control, 1994, pp. 16–21.
[34] Y.C. Chen, C.C. Teng, A model reference control structure using a fuzzy neural network, Fuzzy Sets and Systems 73 (1995) 291–312.
[35] J. Zhang, A.J. Morris, Fuzzy neural networks for nonlinear systems modelling, IEE Proceedings of Control Theory and Applications 6 (142) (1995) 551–556.
[36] T.S.R. Jang, C.T. Sun, Neural-fuzzy modelling and control, Proceedings of IEEE 3 (83) (1995) 378–405.
[37] R.F. Fung, J.S. Huang, J.Y. Yeh, Nonlinear dynamic stability of a moving string by Hamiltonian formulation, Computers & Structures 66 (5) (1998) 597–612.
[38] N.S. Abhyankar, E.K. Hall, S.V. Hanagud, Chaotic vibrations of beams: numerical solution of partial differential equations, American Society of Mechanical Engineers, Journal of Applied Mechanics 60 (1993) 167–174.